A Surface-Charge Study on Cellular-Uptake Behavior of F3-Peptide-Conjugated Iron Oxide Nanoparticles

*Yu Zhang, Mo Yang, Ji-Ho Park, Jennifer Singelyn, Huiqing Ma, Michael J. Sailor, Erkki Ruoslahti, Mihrimah Ozkan, and Cengiz Ozkan**

Surface-charge measurements of mammalian cells in terms of Zeta potential are demonstrated as a useful biological characteristic in identifying cellular interactions with specific nanomaterials. A theoretical model of the changes in Zeta potential of cells after incubation with nanoparticles is established to predict the possible patterns of Zeta-potential change to reveal the binding and internalization effects. The experimental results show a distinct pattern of Zeta potential change that allows the discrimination of human normal breast epithelial cells (MCF-10A) from human cancer breast epithelial cells (MCF-7) when the cells are incubated with dextran coated iron oxide nanoparticles that contain tumor-homing F3 peptides, where the tumor-homing F3 peptide specifically bound to nucleolin receptors that are overexpressed in cancer breast cells.

Keywords:
- cellular uptake
- F3 peptide
- iron oxide nanoparticles
- Zeta potential

1. Introduction

Nanoparticles play an important role in current cancer research, and the interaction of cells with nanoparticles is of particular interest. In this study, we investigated the cellular uptake behaviors of F3 peptide conjugated dextran coated iron oxide nanoparticles with normal breast epithelial cells (MCF-10A) and cancer breast epithelial cells (MCF-7) by cell-surface-charge Zeta potential measurements. Iron oxide nanoparticles are the most commonly investigated nanoparticles for current cancer therapeutics and diagnostics based on their unique chemical and magnetic properties[1,2] and their applications include magnetic resonance imaging (MRI),[3–6] targeted drug delivery[7–9] and magnetic intracellular hyperthermia.[10–12] A wide variety of magnetic iron oxide nanoparticle studies have been reported to date, differing in size and type of coating material used, such as dextran, starch, albumin, silicones and poly(ethyleneglycol) (PEG).[1,13,14] Dextran is one of the most common coatings because it has already being used in clinical trials[15] and proven to be long circulating with no measurable reported toxicity.[13,16,17] F3 peptide was first discovered in a screening procedure that used a phage-displayed cDNA library

[*] Dr. Y. Zhang, Prof. C. Ozkan
Department of Mechanical Engineering
University of California at Riverside
Riverside, CA 92521 (USA)
E-mail: cozkan@engr.ucr.edu
Prof. M. Yang
Department of Health Technology and Informatics
The Hong Kong Polytechnic University
Kowloon, Hong Kong (P.R. China)
J.-H. Park, Prof. M. J. Sailor
Department of Chemistry and Biochemistry
Materials Science and Engineering Program
University of California at San Diego
La Jolla, CA 92093 (USA)
J. Singelyn
Department of Bioengineering
University of California at San Diego
La Jolla, CA 92093 (USA)
H. Q. Ma
Department of Bioengineering
University of California at Riverside
Riverside, CA 92521 (USA)
Prof. E. Ruoslahti
Burnham Institute for Medical Research at UCSB
University of California, Santa Barbara
Santa Barbara, CA 93106 (USA)
Prof. M. Ozkan
Department of Electrical Engineering
University of California at Riverside
Riverside, CA 92521 (USA)

DOI: 10.1002/smll.200900520

NANO MICRO small

and combined ex vivo screening on cell suspensions prepared from mouse bone-marrow cells and in vivo screening for homing to HL-60 human leukemia xenografts tumors.[18] It is a 31-amino acid sequence of the N-terminal fragment of human high-mobility group protein 2 (HMGN2). F3 peptide, reported to have cell-penetrating properties, is promising for drug-targeting and gene-therapy applications, since it is taken up by the cells and it is able to carry a payload into the target cell nucleus.[18–24] It was demonstrated in previous studies that FITC-labeled F3 peptide accumulated on the cell surface and then translocated to the nucleus of breast-cancer cells both in vitro and in xenograft studies.[18,22]

The Zeta (ξ) potential, which is the electrostatic potential that exists at the shear plane of a particle, is related to both surface charge and the local environment of the particle. Zeta potential is commonly used as an important parameter in colloid science to understand the colloid electrostatic interactions.[25] Zeta potential has been used in cell biology to study cell adhesion, activation, and agglutination based on cell-surface-charge properties.[26–28] Altankov et al. stated that the Zeta potential might be a critical parameter for cellular interaction.[29] We have reported the Zeta potential measurements of normal breast epithelial cells (MCF-10A) and cancer breast epithelial cells (MCF-7) after incubation with negatively charged untreated iron oxide nanoparticles, as well as cowpea mosaic virus (CPMV) nanoparticles. The different patterns observed between normal and cancer breast cells indicated that Zeta potential measurements could be a feasible tool in describing the interaction between cells and nanoparticles.[30]

In this study, we observe significant and sensitive changes in Zeta potential measurements of normal breast epithelial cells (MCF-10A) and cancer breast epithelial cells (MCF-7) after incubation with F3 peptide conjugated dextran coated iron oxide nanopaticles. Our results suggest that Zeta potential has a great potential for describing the various interactions between different cells and specific nanoparticles as a valuable biological characteristic.

2. Theory and Analysis

The potential distribution around the double layer region is expressed with the Poisson–Boltzmann equation:[25]

$$n_i(x) = n_i^0 \exp\left[\frac{-z_i e\psi}{kT}\right] \tag{1}$$

where n_i is the number of ions of type i per unit volume in the double layer region. $n_i = n_i^0$ when $\psi = 0$. z_i is the valence of ion i. ψ is the potential. Using the Debye–Huckel approximation, Equation (1) is solved. The potential distribution in the double layer is:

$$\psi = \frac{1}{4\pi\varepsilon_0} \cdot \frac{Q}{D(1+\kappa a)} \frac{e^{-\kappa(r-a)}}{r} \tag{2}$$

where Q is cell surface charge, a is the radius of cell, $\kappa = \left(\frac{e^2 n_i^0 z_i^2}{\varepsilon kT}\right)^{1/2}$, ε is the permittivity.

The potential at the shipping plane surface $r = a + 1/\kappa$ gives the Zeta potential ζ. For cell, as the radius a is much larger than the double layer length $1/\kappa$, the zeta potential can be simplified to:

$$\zeta = \frac{Qe^{-1}}{4\pi\varepsilon_0 Da^2} \cdot \frac{1}{\kappa} \tag{3}$$

When nanoparticles are adsorbed at the cell surface they may influence the Zeta potential in two ways. The adsorption characteristics of the ions present will be influenced and the plane of shear will be shifted from the cell surface. The additional free energy is incorporated into the Boltzmann equation[25] and the modified Poisson–Boltzmann equation with nanoparticle adsorption is given below, where $\beta(x)$ measures how the presence of nanoparticles affect the free energy of the ions at a distance from the cell surface.

$$n_i(x) = n_i^0 \exp\left[\frac{-z_i e\psi}{kT} + \beta(x)\right] \tag{4}$$

Equation (4) is then solved in the Debye–Huckel approximation with $\beta(x) = \beta$ (a constant). The assumption is the uniform distribution of nanoparticle in the cell interface.

Zeta potential is the potential at the shifted slipping plane surface $r = a + 1/\kappa_\beta$, where $\kappa_\beta = \kappa\exp\left(\frac{-\beta}{2}\right)$ is the modified Debye–Huckel parameter.

$$\zeta_\beta = \frac{Qe^{-1}}{4\pi\varepsilon_0 Da^2} \cdot \frac{1}{\kappa_\beta} \tag{5}$$

Comparing Equation (3) and Equation (5), the relative zeta potential $|Z| = \zeta_\beta/\zeta_0$ is:

$$|Z| = \exp\left(\frac{\beta}{2}\right) \tag{6}$$

Nanoparticle uptake by cells is considered a two-step process: first is the binding of nanoparticles to the cell surface, followed by the internalization of nanoparticles by the specific endocytosis pathway. In our previous study,[30] when nanoparticles bind onto the negatively charged cell surface with same sign of Zeta potential, which increases the free energy of the ions at a distance from the cell surface, $\beta^{s}_{\text{binding}}$ is positive, that is, $|Z| > 1$. In this study, the F3 peptide-conjugated iron oxide nanoparticles have measured positively charged, which is the opposite sign of Zeta potential compared to cells. When nanoparticles bind onto the cell surface with opposite sign of zeta potential, which decreases the free energy of the ions at a distance from the cell surface, $\beta^{o}_{\text{binding}}$ is negative, that is, $|Z| < 1$. β_{int} is positive, that is, $|Z| > 1$, during the internalization of nanoparticles by the endocytosis pathway, the position of the plane of shear is shifted and the negative surface charge is increased compared to the binding process. The relative Zeta potential of cells during the adsorption of nanoparticles is expressed as:

$$|Z| = \exp\left(m_{\text{binding}} \cdot \frac{\beta_{\text{bindng}}}{2} + m_{\text{int}} \cdot \frac{\beta_{\text{int}}}{2}\right) \tag{7}$$

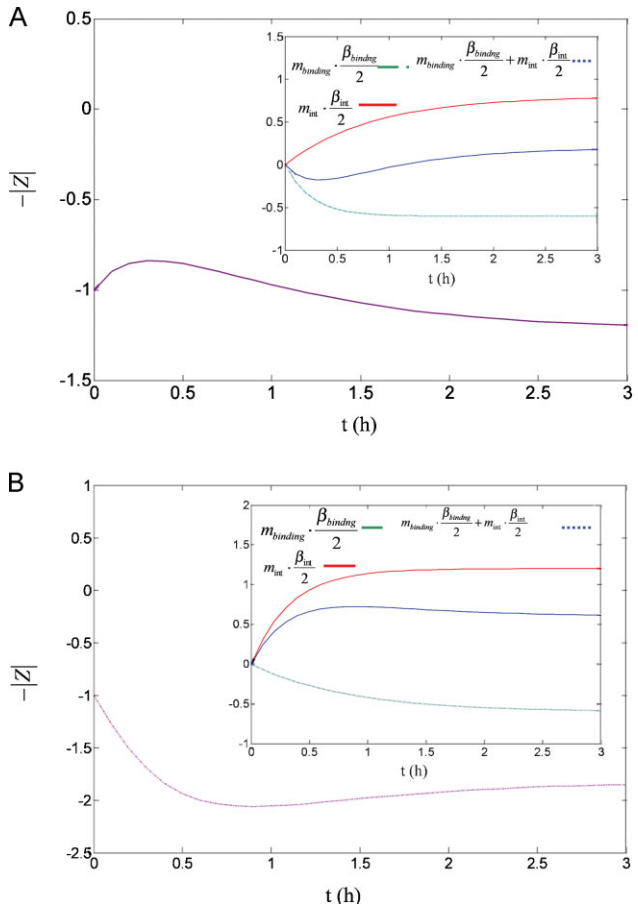

Figure 1. Theoretical evaluation of cells Zeta-potential change versus time after incubation with cationic nanoparticles. A) The binding effect dominates in the first stage and then internalization effect dominates; B) the internalization effect dominates all the time. Insets show stepwise calculations including the individual binding effect, individual internalization effect, and the combination of the two effects. $-|Z|$ has the same trend of real Zeta potential ξ change as the Zeta potential of cells is negative.

where $m_{binding}$ is the total mass of nanoparticles binding to the cell surface; m_{int} is the total mass of nanoparticles internalized within the cell. The binding and internalization processes could be modeled by Langmuir adsorption.[30,31]

The simulation of cell Zeta potential change after incubation with nanoparticles having the same sign of Zeta potential has been discussed before.[30] In this model, cell Zeta potential change after incubation with nanoparticles having opposite sign of Zeta potential is explored under the effect of binding and internalization process, where cells have negative Zeta potential while the nanoparticles have positive Zeta potential. Here, the relative Zeta potential $|Z|$ before nanoparticle incubation is normalized to 1.

The Zeta potential response of cells during the nanoparticle endocytosis is affected by both the binding and internalization effects. In Figure 1A, when the binding effect dominates first and the internalization effect plays a more important role in the following stage, the negative cell Zeta potential ξ will first increase with time and then decrease. In Figure 1B, when the internalization effect dominates during the whole adsorption process, the negative cell Zeta potential ξ will decrease to a stable stage.

3. Results and Discussion

3.1. TEM and SEM Images of F3-Peptide-Conjugated Dextran-Coated Iron Oxide Nanoparticles

Figure 2A shows the schematic illustration of one F3 peptide-conjugated dextran-coated iron oxide nanoparticle. Several iron oxide cores are embedded in the dextran coating and F3 peptides are then conjugated on the surface. FITC attaches to F3 peptide and acts as a probe for nanoparticles to track the cellular uptake behavior of the nanoparticles. Transmission electron microscopy (TEM) and scanning electron microscopy (SEM) images of the iron oxide nanoparticles are shown in Figure 2B. TEM only shows the iron oxide cores of the nanoparticles. The average hydrodynamic diameter of compound nanoparticles was determined by dynamic light scattering (DLS) to be 50.3 nm. Their Zeta potential value measured at pH 7.4 in Hepes buffer is $+10.59 \pm 0.14$ mV.

3.2. Confocal Microscopy Analysis of F3-Peptide-Conjugated Iron Oxide Nanoparticles After Incubation with MCF-7 Cancer Cells and MCF-10A Normal Cells

Nucleolin is confirmed to be a receptor molecule and acts as a shuttle protein that traffics between membrane, cytoplasm, and nucleus.[22–24] Nucleolin expression is usually higher in tumor cells than in normal cells.[32–35] Moreover, the expression level and localization of nucleolin in MCF-7 cells and MCF-10A cells have been studied by Soundararajan et al.[35] Compared with MCF-10A cells, nucleolin is overexpressed in the cytoplasm and present on the cell surface of MCF-7 cells.[32,35]

For the F3 peptide-conjugated iron oxide nanoparticles, the tumor-homing F3 peptide conjugated on the nanoparticle surface specifically bind to nucleolin, which is overexpressed in

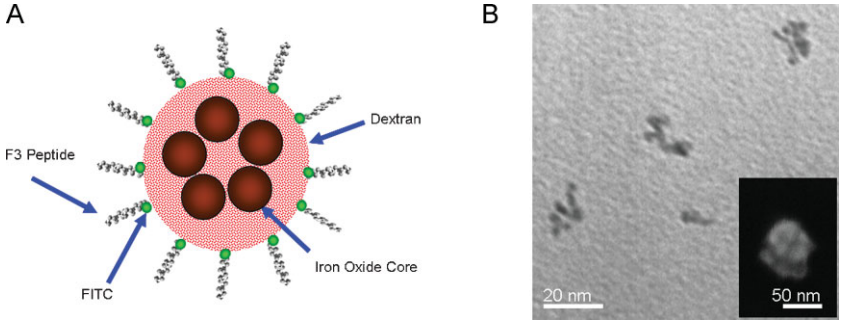

Figure 2. A) Schematic illustration of the structure for F3 peptide-conjugated dextran-coated iron oxide nanoparticles. B) TEM image of iron oxide cores of the nanoparticles. Inset shows SEM image of a single F3 peptide-conjugated dextran-coated iron oxide nanoparticle.

NANO MICRO small

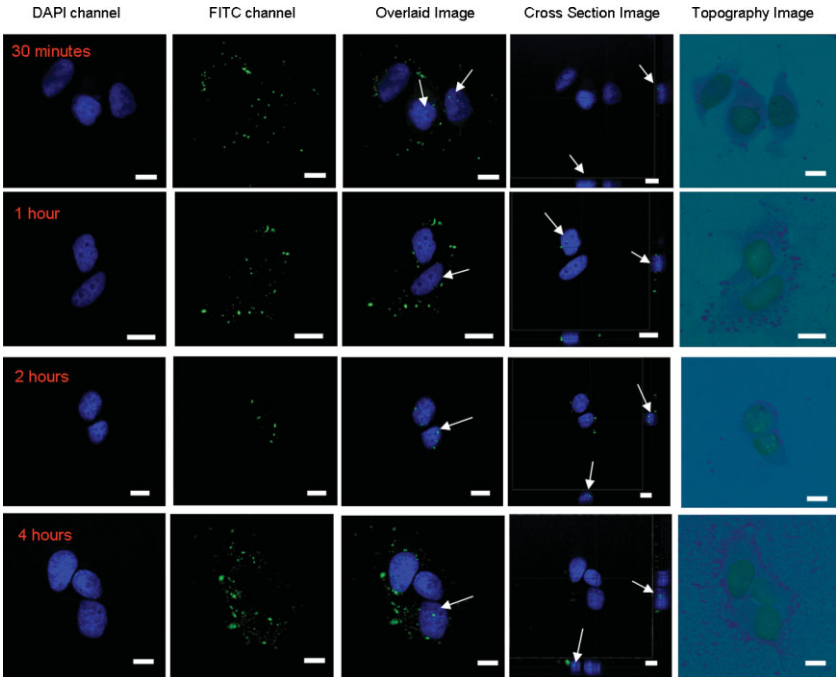

Figure 3. Confocal microscopy analysis of MCF-7 breast cancer cells after incubation with 40 μgFe/mL F3 peptide conjugated iron oxide nanoparticles after 30 minutes, 1 hour, 2 hours, and 4 hours. Leica SP2 Confocal Microscope with a 63× objective was used for imaging. Single DAPI channel, single FITC channel, overlaid image, cross-section image and topography image obtained from Confocal z-series images are showed. For the cross-section image, the large panel is the *x–y* section, the small panel at the bottom is the *x–z* section, and the small panel on the right is the *y-z* section. The nanoparticles are visualized in green by FITC and nuclei are visualized in blue by DAPI counterstaining. The scale bar represents 10 μm. The white arrows point out some of the F3 peptide-conjugated iron oxide nanoparticles that were delivered into the nuclei of MCF-7 cells.

breast carcinoma cells and the degree of internalization is enhanced by the number of F3 peptides attached on the nanoparticles.[36,37] For this study, it is expected that F3 peptide conjugated on the iron oxide nanoparticles could also target overexpressed nucleolin in MCF-7 cells and enhance their internalization of these nanoparticles.

Figure 3 shows the confocal microscopy analysis of MCF-7 cancer breast epithelial cells after incubation with 40 μgFe/mL FITC attached F3 peptide-conjugated iron oxide nanoparticles for different time lengths of 30 minutes, 1 hour, 2 hours, and 4 hours. Single DAPI channel, single FITC channel, overlaid image, cross-section image and topography image obtained from confocal Z series images are showed. The nanoparticles are visualized in green by attached FITC and nuclei are visualized in blue by DAPI counterstaining. From the confocal images, we observed that F3 peptide-conjugated iron oxide nanoparticles are actively uptaken by MCF-7 cancer breast epithelial cells. Most important, although F3 peptide-conjugated iron oxide nanoparticles were only incubated with MCF-7 cells for 30 minutes, nanoparticles have already been internalized and delivered into the nuclei. The overexpressed nucleolin in cancer breast cells is hypothesized to be responsible for the fast internalization and significant amount delivery of F3 peptide-conjugated iron oxide nanoparticles into the nuclei of MCF-7 cells.

Figure 4 shows the confocal microscopy analysis of FITC attached F3 peptide-conjugated iron oxide nanoparticles after incubation with MCF-10A normal breast epithelial cells for different time lengths of 30 minutes, 1 hour, 2 hours, and 4 hours. Internalization of F3 peptide-conjugated iron oxide nanoparticles are also observed for MCF-10A cells over time. Although the F3 peptide uptake pathway for MCF-10A cells is not clear, F3 is rich in basic amino acids and heparan sulfate proteoglycans may act as non-specific receptors for cationic macromolecules.[24,38] Compared to MCF-7 cancer breast cells, not a significant number of F3 conjugated iron oxide nanoparticles were delivered into the nuclei of MCF-10A normal cells, which indicates a lack of nucleolin both on the cell surface and cytoplasm as a shuttle protein compared to cancer breast cells. From the previous study we did,[30] untreated iron oxide nanoparticles didn't enter the cell nucleus after incubation, which explained the different cellular uptake behavior of F3 peptide-conjugated nanoparticles for MCF-10A and MCF-7 cells.

3.3. Zeta-Potential Measurements for Normal and Cancer Cells

Figure 5 reveals the changes of Zeta-potential measurements for both MCF-10A normal breast epithelial cells and MCF-7 cancer breast epithelial cells after incubation with F3 peptide-conjugated dextran-coated iron oxide nanoparticles over time. The Zeta potential of MCF-10A and MCF-7 cells after incubation with dextran-coated iron oxide nanoparticles without conjugation of F3 peptide was measured as the negative control. The Zeta potential of MCF-10A normal cells alone was -31.16 ± 1.12 mV and the Zeta potential of MCF-7 cancer cells alone was -20.32 ± 2.43 mV. The Zeta potential of F3 peptide-conjugated dextran-coated iron oxide nanoparticles has an opposite sign to cells and was measured to be $+10.59 \pm 0.14$ mV. The results of Zeta-potential measurements of MCF-7 and MCF-10A cells after incubation with F3 peptide-conjugated iron oxide nanoparticles exhibit very different trends.

A theoretical basis for the modulation of Zeta potential via nanoparticle incubation is provided in Section 2. Nanoparticle uptake by the cells is explained with a two-step process: a binding process, followed by an internalization process. The attachment of positively charged nanoparticles on the cell plasma membrane will cause the Zeta potential to become intuitively more positive. The internalization process will result in the change of Zeta potential to an opposite way, mainly due to the vesicular-transport-based cell endocytosis. In Figure 5, for MCF-10A cells, the most likely increase of measured

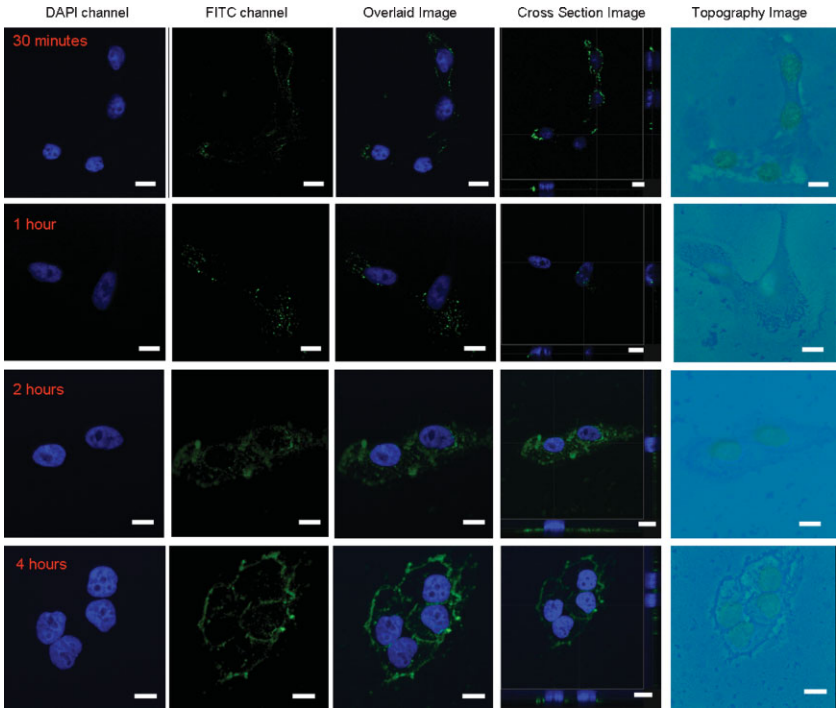

Figure 4. Confocal microscopy analysis of MCF-10A normal breast cells after incubation with 40 μgFe/mL F3 peptide-conjugated iron oxide nanoparticles after 30 minutes, 1 hour, 2 hours, and 4 hours. Leica SP2 Confocal Microscope with a 63× objective was used for imaging. Single DAPI channel, single FITC channel, overlaid image, cross-section image and topography image obtained from Confocal *z*-series images are shown. For the cross-section image, the large panel is the *x*–*y* section, the small panel at the bottom is the *x*–*z* section, and the small panel on the right is the *y*–*z* section. The nanoparticles are visualized in green by FITC and nuclei are visualized in blue by DAPI counterstaining. The scale bar represents 10 μm.

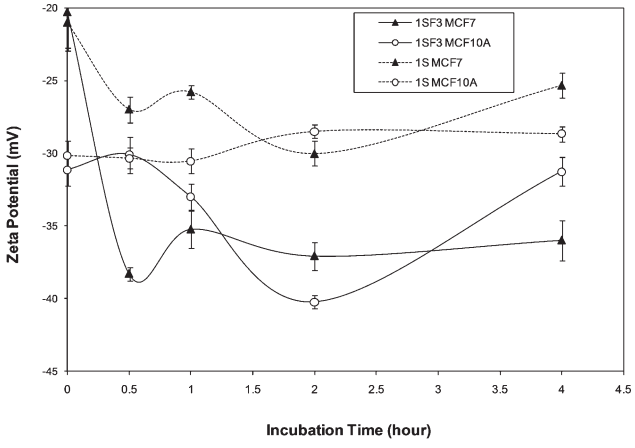

Figure 5. Summary of Zeta-potential changes for MCF-10A normal breast cells and MCF-7 cancer breast cells after incubation with iron oxide nanoparticles with/without conjugation of F3 peptide for 30 minutes, 1 hour, 2 hours, and 4 hours. All the Zeta-potential values were measured using a ZetaPALS system in Hepes buffer (concentration 40 mM, pH 7.4). Note: In the graph, 1SF3 stands for F3 peptide-conjugated dextran coated iron oxide nanoparticles, 1S stands for same-batch-synthesized dextran-coated iron oxide nanoparticles without conjugation of F3 peptide, and the error bar indicates the standard error for 8 runs of Zeta-potential measurements.

Zeta potential after 30 minutes of incubation with F3 peptide-conjugated iron oxide nanoparticles indicates the binding of cationic nanoparticles on the cell surface. The measured Zeta-potential values of MCF-10A cells continuously decreased after incubation with F3 peptide-conjugated dextran-coated iron oxide nanoparticles for 1 hour and 2 hours, which indicates that the internalization effect of F3 peptide-conjugated iron oxide nanoparticles starts to dominate the change of Zeta potential value. After 4 hours, the Zeta potential of MCF-10A cells increased. The possible reason might be that the excytosis effect starts to dominate, which indicates the escape of cationic F3 peptide-conjugated iron oxide nanoparticles. The change of Zeta potential of MCF-10A normal breast cells basically follows the simulated Zeta potential change pattern after incubation with opposite sign nanoparticles that we discussed before. The binding effect dominates first and the internalization effect plays a more important role in the following stage for MCF-10A cells.

In the case of MCF-7 cells, only after 30 minutes of incubation with F3 peptide-conjugated iron oxide nanoparticles, the measured Zeta potential dropped significantly, which indicates that MCF-7 cells internalize the F3 peptide-conjugated nanoparticles quickly due to the overexpressed nucleolin receptors. As F3 peptide tends to bind much faster with overexpressed nucleolin on MCF-7 cancer breast cells than non-specific binding in the case of MCF-10A normal cells, Zeta potential of MCF-7 cells drops much faster than MCF-10A cells. After one-hour incubation with F3 peptide-conjugated iron oxide nanoparticles, the much smaller fluctuation of Zeta potential change for MCF-7 cancer cells possibly due to the overexpressed nucleolin in the cell cytoplasm and the significant amount of nuclei delivery of F3 peptide-conjugated nanoparticles. The Zeta-potential change of MCF-7 cancer cells basically follows the simulated Zeta-potential change pattern after incubation with opposite-sign nanoparticles when the internalization effect dominates during the whole process.

The Zeta potential of dextran-coated iron oxide nanoparticles without conjugation of F3 peptide has the same sign with cells and was measured to be -39.90 ± 0.89 mV. The Zeta-potential changes of MCF-7 cancer cells and MCF-10A normal cells after incubation with only dextran-coated iron oxide nanoparticles are consistent with our previous studies using untreated negatively charged nanoparticles.[30] A much weaker internalization effect is observed in MCF-7 cancer cells for iron oxide nanoparticles without conjugation of F3 peptide, which indicates the role of F3 peptide in binding overexpressed nucleolin in MCF-7 cancer breast cells.

NANO MICRO small

4. Conclusions

In summary, we investigated the different cellular uptake behaviors of F3 peptide-conjugated dextran-coated iron oxide nanoparticles in terms of cell Zeta-potential change for cancer breast epithelial cells (MCF-7) and normal breast epithelial cells (MCF-10A). The overexpressed nucleolin in cancer breast cells is hypothesized to enable the fast internalization compared to normal breast cells and also acts as a shuttle to deliver F3 peptide conjugated nanoparticles into the cell nuclei. The distinct Zeta-potential change patterns of MCF-7 cancer breast cells and MCF-10A normal breast cells after incubation with F3-conjugated nanoparticles demonstrate a sensitive and applicable method for describing the interaction between specific nanoparticles and biological cells. This suggests that a great potential for the surface Zeta-potential measurements to be a promising approach in studying cellular interaction of nanomaterials and open the door for creating a combinatorial label-free approach to quickly identify and monitor the dynamic cell responses in biomedical research.

5. Experimental Section

F3 peptide-conjugated iron oxide nanoparticle synthesis: Iron salts, 0.63 g of $FeCl_3 \cdot 6H_2O$ and 0.25 g $FeCl_2 \cdot 4H_2O$, were mixed with 4.5 g dextran (Sigma) in 10 mL of Millipore water. This acidic solution was neutralized by the dropwise addition of 1 mL of concentrated aqueous ammonia under vigorous stirring and a steady purge of nitrogen, and it was then heated at ~70 °C for 1 h. After purification by centrifuge filtering column (100000 MWCO, Millipore), the magnetic colloid was crosslinked in strong base (5 M aqueous NaOH solution) with epichlorohydrin (Sigma) for 24 h. The colloidal solution was then dialyzed against water for 24 h and filtered through a 0.1-μm-pore-diameter membrane (Millipore). Separation, using a MACS Midi magnetic separation column (Miltenyi Biotec), created two groups of particles with a small (particles going through the magnetic column due to their weak magnetic properties) or a large (particles tapped on the magnetic column due to their strong magnetic properties) size distribution. The group of particles with a small size distribution was used in this study. Amines were then attached to dextran-coated surface of the particles by mixing with aqueous ammonia at room temperature for 48 h and rinsed with the desalting column (GE healthcare). The F3 peptide (KDEPQRRSARLSAKPAPPKPEPKPK-KAPAKK) with cysteine residue added for conjugation and FITC label was synthesized and conjugated to the aminated particles via the short crosslinker Sulfo-SMCC (Pierce).

Particle characterization using TEM, SEM, and DLS: For TEM imaging, an aliquot of F3 peptide-conjugated iron oxide nanoparticles was dropped on to the carbon film on a 200-mesh copper grid and air dried. Nanoparticles were imaged employing a TEM Tecnai12 at the Central Facility for Advanced Microscopy and Microanalysis (CFAMM) in the University of California, Riverside. Nanoparticles were also imaged using a SEM Leo SUPRA 55 at Center for Nanoscale Science and Engineering (CNSE) in the University of California, Riverside. For hydrodynamic size measurements, DLS measurements were performed using a Malvern (Worcestershire, UK) Zetasizer ZS90.

Cell culture: MCF-7 cancer breast epithelial cells and MCF-10A normal breast epithelial cells were purchased from American Type Culture Collection (Rockville, MD). MCF-7 cells were grown in Dulbecco's modified Eagle's medium supplemented with 10% fetal bovine serum, 5% penicillin streptomycin glutamine and 5% sodium pyruvate. MCF-10A cells were grown in mammary epithelial cell medium (Cambrex) supplemented with 100 ng/mL cholera toxin. Cells were all cultured at 37 °C in a humidified and 5% CO_2 atomosphere.

Zeta-potential measurements: 40 μgFe/mL with/without F3 peptide-conjugated iron oxide nanoparticles were incubated with MCF-7 cancer breast epithelial cells and MCF-10A normal breast epithelial cells separately in 25 cm^2 flask at 37 °C in a humidified and 5% CO_2 atomosphere for specified time periods of 30 minutes, 1 hour, 2 hours, and 4 hours. After the incubation procedure, cells were washed three times with 1X Dulbecco's phosphate buffered saline (DPBS). MCF-10A cells were lifted off using 0.05% Typsin-EDTA (GIBCO, Invitrogen) and MCF-7 cells were lifted off using cell dissociation buffer (GIBCO, Invitrogen). After that, they were pelleted down and suspended into Hepes buffer (concentration 40 mM, pH 7.4) for Zeta-potential measurements. The Zeta potential of all the samples was determined with a Zeta Potential Analyzer (ZetaPALs) from Brookhaven Instruments Corporation. Measurements were recorded at 25 °C suspended in Hepes buffer with a Ag electrode using Phase Analysis Light Scattering mode. The Zeta potential was automatically calculated from electrophoretic mobility based on the Smoluchowski equation, $v = (\varepsilon E/\eta)\xi$, where v is the measured electrophoretic velocity, η is the viscosity, ε is the electrical permittivity of the electrolytic solution, and E is the electric field.

Confocal microscopy analysis: Cells were first seeded onto 4-well chamber slides (Lab-Tek™, Nunc). After incubation at 40 μgFe/mL 37 °C with F3 peptide-conjugated iron oxide nanoparticles, cells were washed with 1X DPBS extensively for three times and then fixed with 1% formaldehyde for 30 minutes at room temperature. After being washed with 1X PBS three times and stained with 4′-6-diamidino-2-phenylindole (DAPI), cells were finally mounted on glass slides (Shur/Mount, Water Based mounting media, Electron Microscopy Sciences) after the media chamber and gasket were removed. Confocal z-series images were obtained with a Leica TCS SP2 UV confocal microscope (Wetzlar, Germany) equipped with a 63 × 1.2 NA water objective. To avoid cross excitation, multiple channel images were acquired by scanning in sequential mode. FITC excitation was achieved with a 488-nm Argon laser source and DAPI excitation was achieved with a Coherent UV laser 351 & 364 nm source. Images were processed with Leica Confocal Software (LCS Lite, 2.61).

Acknowledgements

Financial support for this project provided by the Center of Excellence of Nanotechnology for the Treatment, Understanding, and Monitoring of Cancer (NANO-TUMOR) funded by the National Cancer Institute (NCI) is gratefully acknowledged. We

thank Dr. David Carter of The Center for Plant Cell Biology at the University of California, Riverside for technical assistance in confocal imaging.

[1] A. K. Gupta, M. Gupta, *Biomaterials* **2005**, *26*, 3995–4021.
[2] C. C. Berry, A. S. G. Curtis, *J. Phys. D Appl. Phys.* **2003**, *36*, R198–R206.
[3] S. Kubaska, D. V. Sahani, S. Saini, P. F. Hahn, E. Halpern, *Clin. Radiol.* **2001**, *56*, 410–415.
[4] T. Atanasijevic, M. Shusteff, P. Fam, A. Jasanoff, *P. Natl. Acad. Sci. USA* **2006**, *103*, 14707–14712.
[5] P. Smirnov, E. Lavergne, F. Gazeau, M. Lewin, A. Boissonnas, B. T. Doan, B. Gillet, C. Combadiere, B. Combadiere, O. Clement, *Magn. Reson. Med.* **2006**, *56*, 498–508.
[6] F. Cengelli, D. Maysinger, F. Tschudi-Monnet, X. Montet, C. Corot, A. Petri-Fink, H. Hofmann, L. Juillerat-Jeanneret, *J. Pharmacol. Exp. Ther.* **2006**, *318*, 108–116.
[7] A. K. Gupta, S. Wells, *IEEE T. Nanobiosci.* **2004**, *3*, 66–73.
[8] C. Alexiou, W. Arnold, R. J. Klein, F. G. Parak, P. Hulin, C. Bergemann, W. Erhardt, S. Wagenpfeil, A. S. Lubbe, *Cancer Res.* **2000**, *60*, 6641–6648.
[9] T. K. Jain, M. A. Morales, S. K. Sahoo, D. L. Leslie-Pelecky, V. Labhasetwar, *Mol. Pharm.* **2005**, *2*, 194–205.
[10] I. Hilger, K. Fruhauf, W. Andra, R. Hiergeist, R. Hergt, W. A. Kaiser, *Acad. Radiol.* **2002**, *9*, 198–202.
[11] M. Babincova, D. Leszczynska, P. Sourivong, P. Babinec, *Med. Hypotheses* **2000**, *54*, 177–179.
[12] F. Sonvico, S. Mornet, S. Vasseur, C. Dubernet, D. Jaillard, J. Degrouard, J. Hoebeke, E. Duguet, P. Colombo, P. Couvreur, *Bioconjugate Chem.* **2005**, *16*, 1181–1188.
[13] L. M. Lacava, Z. G. M. Lacava, R. B. Azevedo, S. B. Chaves, V. A. P. Garcia, O. Silva, F. Pelegrini, N. Buske, C. Gansau, M. F. Da Silva, P. C. Morais, *J. Magn. Magn. Mater.* **2002**, *252*, 367–369.
[14] L. Babes, B. Denizot, G. Tanguy, J. J. Le Jeune, P. Jallet, *J. Colloid Interf. Sci.* **1999**, *212*, 474–482.
[15] M. G. Harisinghani, S. Saini, R. Weissleder, E. F. Halpern, W. Schima, D. L. Rubin, A. E. Stillman, G. T. Sica, W. C. Small, P. F. Hahn, *Radiology* **1997**, *202*, 687–691.
[16] A. Moore, E. Marecos, A. Bogdanov, R. Weissleder, *Radiology* **2000**, *214*, 568–574.
[17] C. C. Berry, S. Wells, S. Charles, G. Aitchison, A. S. G. Curtis, *Biomaterials* **2004**, *25*, 5405–5413.
[18] K. Porkka, P. Laakkonen, J. A. Hoffman, M. Bernasconi, E. Ruoslahti, *Proc. Natl. Acad. Sci. USA* **2002**, *99*, 7444–7449.
[19] M. E. Akerman, W. C. W. Chan, P. Laakkonen, S. N. Bhatia, E. Ruoslahti, *P. Natl. Acad. Sci. USA* **2002**, *99*, 12617–12621.
[20] E. Ruoslahti, *Biochem. Soc. T.* **2004**, *32*, 397–402.
[21] E. Ruoslahti, T. Duza, L. Zhang, *Curr. Pharm. Design* **2005**, *11*, 3655–3660.
[22] S. Christian, J. Pilch, M. E. Akerman, K. Porkka, P. Laakkonen, E. Ruoslahti, *J. Cell Biol.* **2003**, *163*, 871–878.
[23] J. Enback, P. Laakkonen, *Biochem. Soc. T.* **2007**, *35*, 780–783.
[24] G. R. Reddy, M. S. Bhojani, P. McConville, J. Moody, B. A. Moffat, D. E. Hall, G. Kim, Y. E. L. Koo, M. J. Woolliscroft, J. V. Sugai, T. D. Johnson, M. A. Philbert, R. Kopelman, A. Rehemtulla, B. D. Ross, *Clin. Cancer Res.* **2006**, *12*, 6677–6686.
[25] R. J. Hunter, *Zeta Potential in Colloid Science Principles and Applications*, Academic Press Inc, 1981.
[26] B. Veronesi, C. de Haar, L. Lee, M. Oortgiesen, *Toxicol. Appl. Pharm.* **2002**, *178*, 144–154.
[27] A. Fontes, H. P. Fernandes, M. L. Barjas Castro, A. A. de Thomaz, L. Y. Pozzo, L. C. Barbosa, C. L. Cesar, *Microsc. Microanal.* **2006**, *12*, 1758–1759.
[28] D. Q. Lin, L. N. Zhong, S. J. Yao, *Biotechnol. Bioeng.* **2006** *95*, 185–191.
[29] G. Altankov, K. Richau, T. Groth, *Materialwiss. Werkst.* **2003**, *34*, 1120–1128.
[30] Y. Zhang, M. Yang, N. G. Portney, D. X. Cui, G. Budak, E. Ozbay, M. Ozkan, C. S. Ozkan, *Biomed. Microdevices* **2008**, *10*, 321–328.
[31] C. Wilhelm, F. Gazeau, J. Roger, J. N. Pons, J. C. Bacri, *Langmuir* **2002**, *18*, 8148–8155.
[32] Y. Otake, S. Soundararajan, T. K. Sengupta, E. A. Kio, J. C. Smith, M. Pineda–Roman, R. K. Stuart, E. K. Spicer, D. J. Fernandes, *Blood* **2007**, *109*, 3069–3075.
[33] M. Derenzini, V. Sirri, D. Trere, R. L. Ochs, *Lab. Invest.* **1995**, *73*, 497–502.
[34] A. Pich, L. Chiusa, E. Margaria, *Micron* **2000**, *31*, 133–141.
[35] S. Soundararajan, W. W. Chen, E. K. Spicer, N. Courtenay–Luck, D. J. Fernandes, *Cancer Res.* **2008**, *68*, 2358–2365.
[36] J. H. Park, G. von Maltzahn, L. L. Zhang, M. P. Schwartz, E. Ruoslahti, S. N. Bhatia, M. J. Sailor, *Adv. Mater.* **2008**, *20*, 1630–1635.
[37] G. R. Reddy, M. S. Bhojani, P. McConville, J. Moody, B. A. Moffat, D. E. Hall, G. Kim, Y. E. L. Koo, M. J. Woolliscroft, J. V. Sugai, T. D. Johnson, M. A. Philbert, R. Kopelman, A. Rehemtulla, B. D. Ross, *Clin. Cancer Res.* **2006**, *12*, 6677–6686.
[38] I. A. Khalil, K. Kogure, H. Akita, H. Harashima, *Pharmacol. Rev.* **2006**, *58*, 32–45.

Received: March 25, 2009
Published online: June 24, 2009

